



# Defect configuration and phase stability of cubic versus tetragonal yttria-stabilized zirconia

Hepeng Ding, Anil V. Virkar, Feng Liu \*

Department of Materials Science and Engineering, University of Utah, Salt Lake City, Utah 84112, USA

## ARTICLE INFO

### Article history:

Received 14 October 2011

Received in revised form 20 January 2012

Accepted 12 March 2012

Available online 4 April 2012

### Keywords:

YSZ

DFT

Defect

Phase transition

## ABSTRACT

Using first-principles calculations, we have carried out a systematic comparative study of the microscopic atomic defect configurations in cubic and tetragonal yttria-stabilized zirconia (YSZ) and their correlation with the macroscopic lattice parameters and relative phase stability, as a function of Y concentration. We found that Y atoms sit at the second-nearest-neighbor cation sites to oxygen vacancies and repel each other; oxygen vacancies form pairs and these pairs repel each other. Using the optimized defect configurations as inputs, we correctly identify the experimentally observed tetragonal to cubic transition point and predict the changes of lattice parameters with the increasing Y concentration, in excellent agreement with experiment. Our studies reveal an interesting correlation between the microscopic atomic defect configuration and macroscopic lattice properties.

© 2012 Elsevier B.V. All rights reserved.

## 1. Introduction

YSZ is the most commonly used electrolytes in solid oxide fuel cells (SOFC) for its high ionic and low electronic conductivity. Pure zirconia displays a monoclinic structure ( $P2_1/c$ ) up to a temperature of around 1400 K [1], where monoclinic to tetragonal ( $P4_2/nmc$ ) transition occurs. The cubic ( $Fm3m$ ) phase exists at temperatures higher than 2600 K [2]. The addition of yttria introduces oxygen vacancies for charge compensation, and stabilizes the tetragonal and cubic phases at low temperatures [3,4]. Although the ionic conductivity of YSZ is attributed to the presence of oxygen vacancies introduced by Y doping, it does not simply increase monotonically with the increasing Y concentration but instead displays a maximum at the 15%–18% Y concentration [5]. This interesting behavior of ionic conductivity is ascribed to the change of atomic configurations of YSZ as a function of Y concentration. In particular, two possible reasons are identified: (1) too high an oxygen vacancy concentration leads to the formation of high activation energy pathways for oxygen diffusion [6,7], and (2) the formation of ordered oxygen vacancy complexes at high Y concentrations hinders the vacancy mobility [8]. It has become evident that the atomic defect configuration of Y and oxygen vacancy complexes have a profound effect on the oxygen diffusion and transport in YSZ, and hence on the efficiency of SOFC. Furthermore, the defect configuration is expected to be correlated with the phase stability of different YSZ phases, especially the cubic and tetragonal phases stabilized upon Y doping. Therefore, a detailed study of the defect

configuration and phase stability of cubic versus tetragonal YSZ, as a function of Y concentration, is of both fundamental interest and technological significance.

A great deal of theoretical and experimental work has been dedicated to the defect interactions in cubic YSZ and some work has also been done with respect to the defect configuration in tetragonal YSZ. However, there exist quite some discrepancies in the literature. When  $Y_2O_3$  is added to  $ZrO_2$ , for every two Y atoms replacing two Zr atoms, one oxygen vacancy is created to satisfy charge compensation. Most previous studies found that the oxygen vacancies occupy positions as the second nearest neighbors (2NNs) to the two Y atoms and next to Zr atoms in both cubic and tetragonal YSZ [9–17], while some other studies suggested that the oxygen vacancies prefer to be the NNs [18–22] or 3NNs to the Y atoms [23], or change their preferred sites with changing Y concentration [24]. For high Y doping concentrations, some studies found that Y atoms repel each other in cubic YSZ [9] while others suggested attraction between Y [15,23], and Y–Y interaction was suggested to be attractive in tetragonal YSZ [17]. Oxygen vacancies are found to have a tendency to form pairs in cubic YSZ, with a variety of pairing directions suggested, such as  $\langle 1\ 0\ 0 \rangle$  [25],  $\langle \frac{3}{2}\ \frac{1}{2}\ 0 \rangle$  [25],  $\langle 1\ 1\ 1 \rangle$  [8,14,23,26–28],  $\langle 1\ 1\ 2 \rangle$  [29], and  $\langle 1\ \frac{1}{2}\ 0 \rangle$  [30]. One study showed that in tetragonal YSZ, oxygen vacancies repel each other, staying as far as possible [17]. Several papers studied the oxygen pair interactions in cubic YSZ and suggested different alignment directions, such as  $\langle 1\ 1\ 2 \rangle$  [8,29] and  $\langle 1\ \frac{1}{2}\ 0 \rangle$  [14].

In the present study, we revisit the problem of atomic defect configurations in both cubic and tetragonal YSZ. Using extensive first-principles calculations, we examine all the possible defect–defect interactions as a function of Y, including Y– $V_O$  (oxygen vacancy), Y–Y,

\* Corresponding author.

E-mail address: [fliu@eng.utah.edu](mailto:fliu@eng.utah.edu) (F. Liu).

$V_{\delta}-V_{\delta}$ , and  $V_{\delta}V_{\delta}$  pair– $V_{\delta}V_{\delta}$  pair interactions, to identify the most energetically favorable defect configuration. Furthermore, as an independent check of our results, we use the optimized defect configurations as inputs to calculate the relative phase stability of cubic and tetragonal YSZ and their lattice parameters as a function of Y concentration, to facilitate a direct comparison with experiments. We are able to predict the tetragonal to cubic phase transition point with Y doping and the trends of changing lattice parameters of both phases as the Y concentration increases. Our results are in very good agreement with the experiments, which in turn confirms the correctness of the defect configurations we found. Furthermore, our studies reveal an interesting correlation between the microscopic atomic defect configuration and macroscopic lattice properties.

## 2. Computational method

All the calculations are performed using the FHI-aims [31], an ab initio density-functional theory (DFT) code employing all electron basis sets. An fcc-like unit cell containing 4  $ZrO_2$  formulas and a  $2 \times 2 \times 2$  fcc-like supercell containing 32  $ZrO_2$  base formulas are used for modeling  $ZrO_2$  and YSZ, respectively. The energy cutoff and the force criterion used are  $10^{-6}$  eV and  $10^{-4}$  eV/Å, respectively. To ensure convergence, light basis settings for Zr, Y, and additional 4f orbital of tier2 [32] added O, along with a 768 k-point  $\times$  atom mesh are used to give lattice constant variances smaller than  $10^{-2}$  Å and relative phase energy difference variances smaller than 5 meV/formula. For exchange and correlation functional, PW-LDA [33] formula is used. According to our calculation results, it gives better agreement with the experiment [37,38] in terms of relative phase stability for cubic, tetragonal, and monoclinic phases than PBE [34] formula.

## 3. Results and discussion

### 3.1. Lattice and structural properties of $ZrO_2$

As a benchmark of our methods, we first calculated the structural and energetic properties of three pure  $ZrO_2$  phases. For cubic  $ZrO_2$ , only one lattice parameter, the lattice constant  $a$  needs to be optimized, since all the atoms sit in the high-symmetry points of the fcc lattice sites. For tetragonal  $ZrO_2$ , two lattice parameters,  $a$  and  $c$ , and one internal atomic coordinate, the  $z$ -component of O atom, need to be optimized, since the O is displaced from the high-symmetry lattice point along the  $z$ -axis by  $\Delta z$  or in unit of lattice parameter  $c$  as  $dz = \Delta z/c$ . For monoclinic  $ZrO_2$ , four lattice parameters,  $a$ ,  $b$ ,  $c$  and  $\beta$  ( $\beta$  is the angle between  $x$  and  $z$  axils), and nine internal atomic coordinates need to be optimized, since there are three kinds of atoms (Zr,  $O_1$  and  $O_2$ ) all without any symmetry constraint.

Our optimized lowest-energy lattice and structural properties are shown in Table 1, along with the available experimental data and several previous calculation results for comparison. The monoclinic structure is the most stable phase at absolute zero temperature and the specific volume per  $ZrO_2$  formula follows the order of  $V_{\text{cubic}} < V_{\text{tetragonal}} < V_{\text{monoclinic}}$ . In general, our results are in good agreement with the experimental and previous computational results, which validates the method we use.

### 3.2. Defect configurations in cubic and tetragonal YSZ

As Y is doped to substitute Zr in  $ZrO_2$  and accompanied with oxygen vacancies to form YSZ, three basic kinds of defect interactions are introduced, namely,  $V_{\delta}-Y$ ,  $Y-Y$  and  $V_{\delta}-V_{\delta}$  interactions. To find the most stable defect configuration in YSZ, all three interactions need to be examined for energy minimization, and the results are expected to sensitively depend on Y concentration because these interactions shall change with the changing Y concentration. Furthermore, possible change of lattice structure needs also to be considered, because the relative stability of different phases, e.g. cubic and tetragonal

**Table 1**

Calculated and experimental  $ZrO_2$  lattice and structural parameters. Energy of monoclinic phase is set as the reference of zero energy.

Lattice properties	This work	PP LDA [35]	PP LDA [9]	PP LDA [36]	Experiment [37,38]
<i>Cubic</i>					
$a$ (Å)	5.031	5.037	5.078	5.035	5.090
$V$ (Å <sup>3</sup> / $ZrO_2$ )	31.84	32.10	32.73	31.91	32.97
$B_0$ (GPa)	272		268		194–220
$E$ (eV/ $ZrO_2$ )	0.094		0.111	0.102	0.120
<i>Tetragonal</i>					
$a$ (Å)	5.037	5.030	5.087	5.039	5.050
$c$ (Å)	5.112	5.100	5.162	5.104	5.182
$c/a$	1.015	1.014	1.015	1.013	1.026
$dz$	0.043	0.042	0.042	0.042	0.0574
$V$ (Å <sup>3</sup> / $ZrO_2$ )	32.43	32.26	33.39	32.41	33.04
$B_0$ (GPa)	234		197		190
$E$ (eV/ $ZrO_2$ )	0.044		0.063	0.057	0.057
<i>Monoclinic</i>					
$a$ (Å)	5.093	5.108		5.086	5.151
$b$ (Å)	5.176	5.170		5.208	5.212
$c$ (Å)	5.244	5.272		5.226	5.317
$\beta$ (deg)	99.10	99.21		99.21	99.23
$x$ (Zr)	0.2771	0.2769	0.2769	0.2779	0.2754
$y$ (Zr)	0.0421	0.0422	0.0430	0.0418	0.0395
$z$ (Zr)	0.2101	0.2097	0.2100	0.2099	0.2083
$x$ ( $O_1$ )	0.0710	0.0689	0.0640	0.0766	0.0700
$y$ ( $O_1$ )	0.3370	0.3333	0.3237	0.3488	0.3317
$z$ ( $O_1$ )	0.3420	0.3445	0.3524	0.3311	0.3447
$x$ ( $O_2$ )	0.4493	0.4495	0.4497	0.4471	0.4496
$y$ ( $O_2$ )	0.7575	0.7573	0.7560	0.7588	0.7569
$z$ ( $O_2$ )	0.4807	0.4798	0.4790	0.4830	0.4792
$V$ (Å <sup>3</sup> / $ZrO_2$ )	34.13	34.35	35.04	34.16	35.22
$B_0$ (GPa)	267		185		95–189

phases, depends on the internal structure of defect configurations. We have carried out a systematic comparative study of defect configurations in cubic and tetragonal YSZ by calculating all three kinds of defect interactions to determine the most stable defect configurations as a function of Y concentration. Using the optimized lowest-energy defect configuration as inputs, we further validate the results by predicting the Y doping induced phase transition between the cubic and tetragonal phases and changes of lattice parameters with Y concentration, in comparison with the available experimental results.

In what follows, if not specified, the energy is presented as the relative energy in unit of eV/supercell, with the lowest-energy configuration set as the reference of zero energy. For convenience, the notation of  $[a,b,c]$  or  $\langle a,b,c \rangle$  is used to denote not only the direction but also the separation distance along the given lattice axis.

#### 3.2.1. Defect interactions in cubic YSZ

**3.2.1.1. Defect configuration of one basic doping unit:  $V_{\delta}-Y$  and  $Y-Y$  interactions.** Since one oxygen vacancy is created to accompany two doped Y atoms, one considers a  $Y-V_{\delta}-Y$  trimer as the most basic doping unit, whose configuration, involving both  $V_{\delta}-Y$  and  $Y-Y$  interactions, is to be determined first. To study the configuration of one single  $Y-V_{\delta}-Y$  trimer unit, which is the dominating configuration at low Y concentration limit, we introduce one oxygen vacancy and two Y atoms in the supercell, as shown in Fig. 1. First, we examined the  $V_{\delta}-Y$  interactions by changing the distances of two Y atoms from the oxygen vacancy. Around an oxygen vacancy, there are four NN, twelve 2NN and twelve 3NN Zr sites for the two Y atoms to occupy. The relative energies of different occupations are calculated as shown in Table 2. We found that the most stable  $Y-V_{\delta}-Y$  trimer configuration is to have both Y atoms sitting at the 2NN positions to the oxygen vacancy, denoted as the 2NN/2NN configuration in Table 2. The NN/3NN configuration, i.e. with one Y being the NN and the

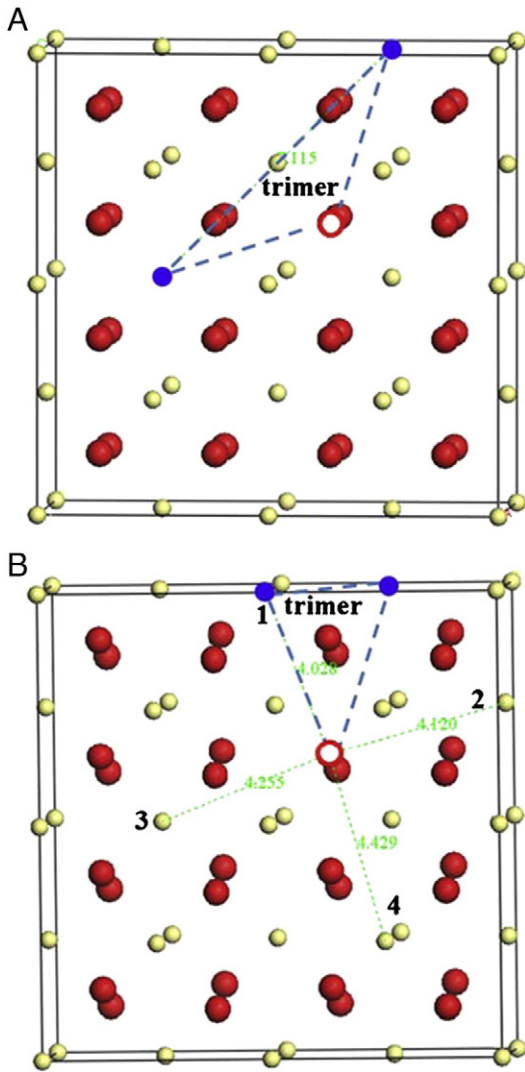


**Fig. 1.** The most stable defect configuration of a Y- $V_{O}$ -Y trimer basic unit in (A) cubic and (B) tetragonal YSZ. Zr atoms are small (yellow) balls, oxygen atoms are large (red) balls, Y atoms are medium (blue) balls, and oxygen vacancy is a (red) open circle. The numbers in (B) mark the different distances of 2NN cation sites to the oxygen vacancy.

other Y being the 3NN to the oxygen vacancy, has the second lowest energy. Our results agree with the majority of previous experimental and theoretical studies [9–16], but disagree with some other studies showing the NN/NN [18–22] or 3NN/3NN [23] to be the lowest-energy configuration.

We believe that the 2NN/2NN preference is due to the balance between electrostatic energy ( $Y^{3+}$  vs.  $Zr^{4+}$ ) and strain energy (the ionic radius  $r(Y^{3+}) = 1.04$  nm [39] is larger than  $r(Zr^{4+}) = 0.86$  nm [39]). In view of the electrostatic energy,  $Y^{3+}$  instead of  $Zr^{4+}$  prefers to stay close to oxygen vacancy to reduce Coulomb energy because oxygen vacancy has a positive effective charge. However, in view of the ionic radius,  $Y^{3+}$  prefers to have more room for its larger size. “Structural relaxation” shows that a cation next to the oxygen vacancy, surrounded by seven oxygen atoms, will have smaller room than a normal cation site, surrounded by eight oxygen atoms without oxygen vacancy. Consequently,  $Y^{3+}$  prefers to stay away from the oxygen vacancy to reduce strain energy. Thus, the competition of these two energies results in the Y atoms sitting at the 2NN cation sites of oxygen vacancy.

Among the twelve 2NN cation sites to oxygen vacancy which are all equivalent in cubic YSZ, the two Y atoms may also arrange differently to

minimize the Y–Y interaction. There are three choices in terms of Y–Y separation, which we denoted in the ascending order of separation as YY-1, YY-2 and YY-3 in Table 2. Clearly, due to Coulomb repulsion, the Y–Y interaction energy decreases with the increasing Y–Y separation, as shown in Table 2. This agrees with Stapper et al. [8] but disagrees with Bogicevia et al. [23] who suggested that Y–Y be attractive with each other favoring the YY-1 positions. Also to be noted that the  $V_{O}$ -Y interaction energies shown in Table 2 as discussed above are results with the minimum Y–Y interaction energy or the largest Y–Y separation for any given  $V_{O}$ -Y separation. Thus, to minimize both  $V_{O}$ -Y and Y–Y interactions, the most stable defect configuration of a Y- $V_{O}$ -Y trimer, the basic doping unit of  $Y_2O_3$  in  $ZrO_2$ , is to have two Y atoms occupying the 2NN cation sites to the oxygen vacancy with the greatest Y–Y separation, as shown in Fig. 1A.

**3.2.1.2. Defect configuration of two doping units:  $V_{O}$ - $V_{O}$  interaction.** As more  $Y_2O_3$  added to  $ZrO_2$ , the distribution of the basic doping unit Y- $V_{O}$ -Y trimer, defines the defect configuration, which is determined by the interactions between the doping units. Keeping the basic Y- $V_{O}$ -Y trimer configuration intact, their interactions can be effectively characterized by the  $V_{O}$ - $V_{O}$  interaction. To study the  $V_{O}$ - $V_{O}$  interaction, we introduce two oxygen vacancies and four Y atoms into the supercell, which corresponds to a 12.5% Y concentration. Within the supercell, there are nine choices of O vacancy separations along different crystallographic directions, denoted as  $\langle \frac{1}{2}, 0, 0 \rangle$ ,  $\langle -\frac{1}{2}, \frac{1}{2}, 0 \rangle$ ,  $\langle \frac{1}{2}, \frac{1}{2}, \frac{1}{2} \rangle$ ,  $\langle 1, 0, 0 \rangle$ ,  $\langle 1, \frac{1}{2}, 0 \rangle$ ,  $\langle 1, \frac{1}{2}, \frac{1}{2} \rangle$ ,  $\langle 1, 1, 0 \rangle$ ,  $\langle 1, 1, \frac{1}{2} \rangle$ , and  $\langle 1, 1, 1 \rangle$  having a separation distance equal to  $0.5a$ ,  $0.707a$ ,  $0.866a$ ,  $a$ ,  $1.118a$ ,  $1.225a$ ,  $1.414a$ ,  $1.5a$ , and  $1.732a$ , respectively, where  $a = 5.031$  Å is the lattice constant. The relative energies of these nine  $V_{O}$ - $V_{O}$  separations are shown in Table 2 with the lowest energy separation  $\langle 1, \frac{1}{2}, \frac{1}{2} \rangle$  set as the reference of zero energy. Interestingly, instead of being separated as far as possible, oxygen vacancies prefer to have the alignment of  $\langle 1, \frac{1}{2}, \frac{1}{2} \rangle$ . Another preferred alignment is  $\langle 1, \frac{1}{2}, 0 \rangle$  which has almost a degenerate energy with  $\langle 1, \frac{1}{2}, \frac{1}{2} \rangle$ . We consider these two lowest-energy alignments of oxygen vacancies as one  $V_{O}V_{O}$  pair.

A large variety of experimental and computational results can be found in literature regarding the oxygen vacancy alignment. In experiment, Dai et al. [25] found that oxygen vacancies have an alignment along  $\langle 1, 0, 0 \rangle$  or  $\langle \frac{3}{2}, \frac{1}{2}, 0 \rangle$  direction, Osborn et al. [26] and Hull et al. [27] found that oxygen vacancies have an ordering along  $\langle \frac{1}{2}, \frac{1}{2}, \frac{1}{2} \rangle$ , and Goff et al. [8] found that oxygen vacancies have an alignment along  $\langle 1, 1, 1 \rangle$ . In theory, our results agree with Predith et al. [29] who found that oxygen vacancies form parallel  $\langle 1, 1, 2 \rangle$  chains by using cluster expansion method combined with DFT. In contrast, Dalach [30] found that oxygen vacancies have a significant ordering along  $\langle 1, \frac{1}{2}, 0 \rangle$  also by using cluster expansion method. Several other papers reported different alignment directions using different computational methods. Bogicevia et al. [23,28] and Ostanin et al. [14] found that oxygen vacancy has an ordering along  $\langle \frac{1}{2}, \frac{1}{2}, \frac{1}{2} \rangle$ , and Fabris et al. [40] found that the clustering of oxygen vacancies align along  $\langle 1, 1, 1 \rangle$ .

**3.2.1.3. Defect configuration of two doping unit pairs:  $V_{O}V_{O}$  pair- $V_{O}V_{O}$  pair interaction.** At even higher Y concentration, multiple interactions between doping units and unit pairs become very complicated. From Tables 2 and 3, we can see that the order of interaction strength goes like  $V_{O}$ - $V_{O}$  ( $\sim 1.00$  eV)  $>$  Y- $V_{O}$ -Y ( $\sim 0.50$  eV)  $>$  Y–Y ( $\sim 0.20$  eV). Therefore, below we will focus on the  $V_{O}$ - $V_{O}$  interaction in the discussion of Y- $V_{O}$ -Y trimer distribution. By treating the unit pair as a whole, we further attempted to study defect configurations at the 25% Y concentration, in terms of  $V_{O}V_{O}$  pair- $V_{O}V_{O}$  pair interaction, by introducing four oxygen vacancies and eight Y atoms into a supercell. We considered the pair-pair alignment and interaction in two ways. First, we set the lowest-energy oxygen vacancy pair of the  $\langle 1, \frac{1}{2}, \frac{1}{2} \rangle$  alignment as the basic interacting units denoted as case 1, and calculated the pair-pair interaction energies as a function of their separation direction and

**Table 2**  
Defect interactions in Cubic YSZ.

$V_{\delta}$ -Y	NN/NN		2NN/2NN	3NN/3NN	NN/2NN	NN/3NN	2NN/3NN		
E (eV)	0.32		0	0.51	0.24	0.08	0.16		
Y-Y	YY-1			YY-2			YY-3		
E (eV)	0.17			0.03			0.00		
$V_{\delta}$ - $V_{\delta}$	$\langle \frac{1}{2}, 0, 0 \rangle$	$\langle \frac{1}{2}, \frac{1}{2}, 0 \rangle$	$\langle \frac{1}{2}, \frac{1}{2}, \frac{1}{2} \rangle$	$\langle 1, 0, 0 \rangle$	$\langle 1, \frac{1}{2}, 0 \rangle$	$\langle 1, \frac{1}{2}, \frac{1}{2} \rangle$	$\langle 1, 1, 0 \rangle$	$\langle 1, 1, \frac{1}{2} \rangle$	$\langle 1, 1, 1 \rangle$
E (eV)	0.41	0.64	0.95	1.17	0.02	0.00	0.71	0.78	0.85
$V_{\delta}V_{\delta}$ pair- $V_{\delta}V_{\delta}$ pair case 1			$\langle 0, \frac{1}{2}, \frac{1}{2} \rangle$	$\langle 1, 0, 0 \rangle$	$\langle 0, \frac{1}{2}, 1 \rangle$	$\langle \frac{1}{2}, 1, \frac{1}{2} \rangle$	$\langle 0, 1, 1 \rangle$		
E (eV)			1.02	0.94	0.72	0.58	0.00		
$V_{\delta}V_{\delta}$ pair- $V_{\delta}V_{\delta}$ pair case 2			$\langle 1, 0, 0 \rangle$	$\langle 1, \frac{1}{2}, 0 \rangle$	$\langle 1, \frac{1}{2}, \frac{1}{2} \rangle$		$\langle 1, 1, 0 \rangle$		
E (eV)			2.31	0.87	0.00		1.51		

distance as listed in Table 2. We found that the  $\langle 1, \frac{1}{2}, \frac{1}{2} \rangle$   $V_{\delta}V_{\delta}$  pairs repel each other, with the interaction energy decreasing with the increasing separation. The system has the lowest energy when the two  $\langle 1, \frac{1}{2}, \frac{1}{2} \rangle$   $V_{\delta}V_{\delta}$  pair is separated by  $\langle 0, 1, 1 \rangle$  which is the largest possible separation in our supercell. In the second case, we assume the  $\langle 0, 1, 1 \rangle$  is the most favorable separation direction as found in case 1 between two oxygen vacancy pairs, and then determine the preferred the alignment of each oxygen pair. We found that at any separation distance along  $\langle 0, 1, 1 \rangle$ , the lowest-energy alignment of  $V_{\delta}V_{\delta}$  pair is the  $\langle 1, \frac{1}{2}, \frac{1}{2} \rangle$ . For example, the two  $\langle 1, \frac{1}{2}, \frac{1}{2} \rangle$   $V_{\delta}V_{\delta}$  pairs interaction energy is much higher than that of two  $\langle 1, \frac{1}{2}, \frac{1}{2} \rangle$   $V_{\delta}V_{\delta}$  pairs along the  $\langle 0, 1, 1 \rangle$ , as shown in Table 2. The same results are also found for the 18.75% Y concentration with three oxygen vacancies and six Y atoms introduced in the supercell (not shown). This indicates that at high Y concentration, the  $\langle 1, \frac{1}{2}, \frac{1}{2} \rangle$   $V_{\delta}V_{\delta}$  pair alignment becomes the only dominant oxygen vacancy pair configuration, even though at low Y concentration the  $\langle 1, \frac{1}{2}, 0 \rangle$  alignment can be present too with almost degenerate energy with the  $\langle 1, \frac{1}{2}, \frac{1}{2} \rangle$  alignment. Such change of preferred  $V_{\delta}V_{\delta}$  pair alignments with Y concentration may have an important effect on the relative phase stability and lattice properties of cubic and tetragonal phases as a function of Y concentration as we will show below.

To summarize the defect interactions in cubic YSZ, the Y- $V_{\delta}$ -Y trimer represents the basic doping unit with Y atoms sitting at the 2NN of oxygen vacancy and repelling each other among themselves; the Y- $V_{\delta}$ -Y trimer units form pairs along the  $\langle 1, \frac{1}{2}, 0 \rangle$  and  $\langle 1, \frac{1}{2}, \frac{1}{2} \rangle$  at low Y concentration, while only the  $\langle 1, \frac{1}{2}, \frac{1}{2} \rangle$  alignment dominates at high Y concentration; the  $\langle 1, \frac{1}{2}, \frac{1}{2} \rangle$   $V_{\delta}V_{\delta}$  pairs align along  $\langle 0, 1, 1 \rangle$  and repel each other. We may compare our results of the  $V_{\delta}V_{\delta}$  pair interactions in cubic YSZ with previous studies. In experiment, Goff et al. [8] found that oxygen vacancy pairs pack together in  $\langle 1\ 1\ 2 \rangle$  directions as Y

concentration increases, which is consistent with our results of preferred  $\langle 1, \frac{1}{2}, \frac{1}{2} \rangle$  alignment. In theory, Predith et al. [29] also found that  $V_{\delta}$ - $V_{\delta}$  pairs order along the  $\langle 1, \frac{1}{2}, \frac{1}{2} \rangle$  direction.

### 3.2.2. Defect interactions in tetragonal YSZ

**3.2.2.1. Defect configuration of a basic doping unit:  $V_{\delta}$ -Y and Y-Y interactions.** In tetragonal YSZ, there exists a lattice asymmetry as the  $c$ -axis is larger than the  $a$ -axis and correspondingly the internal structure exhibits anisotropy in terms of oxygen atomic positions, i.e., the oxygen atoms are displaced along the  $c$ -axis making their  $z$ -coordinates distinguishable from  $x$ - and  $y$ -coordinates. Consequently, the positions of oxygen vacancies upon Y doping and hence the defect configurations have an isotropic preference in choosing the  $z$ -direction alignments from the alignments in the other two directions. Consider the basic doping unit of a Y- $V_{\delta}$ -Y trimer, as found above in the cubic YSZ, with two Y atoms sitting at the 2NN sites to an oxygen vacancy. In the tetragonal YSZ, the twelve 2NN cation sites to the oxygen vacancy are no longer equivalent. As shown in Fig. 1B, two 2NN cation sites have the smallest  $V_{\delta}$ -Y/Zr distance (denoted as 2NN-1), four 2NN cation sites have the second smallest  $V_{\delta}$ -Y/Zr distance (denoted as 2NN-2), another four 2NN cation sites have the second largest  $V_{\delta}$ -Y/Zr distance (denoted as 2NN-3), and two 2NN cation sites have the largest  $V_{\delta}$ -Y/Zr distance (denoted as 4). Among them, the two Y atoms may occupy different sites to minimize the repulsive Y-Y interaction, while at the same time to maximize the attractive  $V_{\delta}$ -Y interactions due to the slightly different 2NN  $V_{\delta}$ -Y distances. Our calculated relative configuration energies are shown in Table 3. Here 11 [YY-1] denotes both Y atoms sit at the 2NN-1 sites having the smallest  $V_{\delta}$ -Y distance while the separation between two Y atoms is YY-1, the smallest. The results in Table 3 indicate that the balance between the Y-Y repulsion and the  $V_{\delta}$ -Y

**Table 3**  
Defect interactions in tetragonal YSZ.

Y-Y	11 [YY-1]	22 [YY-3]	22 [YY-1]	33 [YY-3]	33 [YY-1]	44 [YY-1]	13 [YY-3]	12 [YY-2]	
E (eV)	0.04	0.05	0.15	0.12	0.20	0.29	0.00	0.09	
$V_{\delta}$ - $V_{\delta}$	$[1, 0, 0]$	$[0, 1, 0]$	$[0, 0, 1]$	$[1, 0, \frac{1}{2}]$	$[0, 1, \frac{1}{2}]$	$[1, \frac{1}{2}, 0]$	$[1, \frac{1}{2}, \frac{1}{2}]$	$[\frac{1}{2}, \frac{1}{2}, 1]$	$[1, 1, 1]$
E (eV)	1.44	1.44	1.53	0.19	0.19	0.00	0.14	0.75	0.77
$V_{\delta}V_{\delta}$ pair- $V_{\delta}V_{\delta}$ pair case 1				$[1, \frac{1}{2}, 0]$				$[1, \frac{1}{2}, \frac{1}{2}]$	
E (eV)				0.43				0.00	
$V_{\delta}V_{\delta}$ pair- $V_{\delta}V_{\delta}$ pair case 2			$[\frac{1}{2}, 1, 1]$			$[\frac{1}{2}, 1, \frac{1}{2}]$			
E (eV)			0.63			0.21	0.00		

attraction defines the lowest energy configuration. For the fixed Y–Y separation, the configuration with smaller  $V_{\delta}$ –Y separation is more preferred, for example, E (22 [YY-3]) < E (33 [YY-3]). For the fixed  $V_{\delta}$ –Y distance, the larger the Y–Y distance, the lower the configuration energy, for example, E (22 [YY-3]) < E (22 [YY-1]). Among all possibilities, the 13 [YY-3] and the 11 [YY-1] configurations (as shown in Fig. 1B) have the lowest energy. This finding is consistent with the previous work by Eichler [17].

**3.2.2.2. Defect configuration of two doping units:  $V_{\delta}$ – $V_{\delta}$  interaction.** Similar to the study of cubic YSZ discussed above, we introduce two oxygen vacancies and four Y atoms into the supercell, which corresponds to a 12.5% Y concentration, to study  $V_{\delta}$ – $V_{\delta}$  interaction. As an example, we choose the configuration of two lowest-energy 11 [YY-1] Y– $V_{\delta}$ –Y trimer units in the supercell to study the  $V_{\delta}$ – $V_{\delta}$  (i.e., trimer–trimer) interaction. Table 3 shows the relative energies for several possible oxygen vacancy separations. Unlike Eichler's [17] finding that oxygen vacancies prefer to stay as far as possible without directional preference, our results show that oxygen vacancies in tetragonal YSZ also prefer to form pairs as they do in cubic YSZ, but with different direction of alignment, favoring the  $[1, \frac{1}{2}, 0]$  alignment instead of the  $\langle 1, \frac{1}{2}, \frac{1}{2} \rangle$  alignment in cubic YSZ.

**3.2.2.3. Defect configuration of two doping unit pairs:  $V_{\delta}V_{\delta}$  pair– $V_{\delta}V_{\delta}$  pair interaction.** Given the formation of the  $[1, \frac{1}{2}, 0]$  aligned  $V_{\delta}V_{\delta}$  pairs in tetragonal YSZ, we then studied the  $V_{\delta}V_{\delta}$  pair– $V_{\delta}V_{\delta}$  pair interactions at even high Y concentration. Again, we introduced four oxygen vacancies and eight Y atoms into the supercell corresponding to a 25% Y concentration. Since we have already known from the studies of cubic YSZ that oxygen vacancy pairs repel each other, we first choose the  $[0, 1, 1]$  direction, because it gives the largest pair–pair separation distance, and tested pairs of different alignments, shown as the case 1 in Table 3. Note that in tetragonal lattice, the  $[0, 1, 1]$  direction is longer than the  $[1, 1, 0]$  direction, while in cubic lattice all the  $\langle 0, 1, 1 \rangle$  directions have the same distance. Although the single “isolated”  $V_{\delta}V_{\delta}$  pair favors the  $[1, \frac{1}{2}, 0]$  alignment at low Y concentration, interestingly, we found that the pair–pair interaction changes the preferred pair alignment into  $[1, \frac{1}{2}, \frac{1}{2}]$  direction at high Y concentration, as shown in Table 3. The main reason for such change of oxygen vacancy pair alignment is found to be associated with the change of lattice parameters with the increasing Y concentration. The tetragonal lattice tends to become more cubic like (i.e., decreasing  $c/a$  ratio and decreasing  $dz$ , see more discussion below) at high Y concentration, which converts the oxygen vacancy pair alignment to what has been found in the cubic case, i.e., the  $[1, \frac{1}{2}, \frac{1}{2}]$  alignment. Next, we fix the  $[1, \frac{1}{2}, \frac{1}{2}]$  pair alignment and calculated the interaction energies between two such pairs along different directions, listed as case 2 in Table 3. Again, we found that the  $[0, 1, 1]$  pair–pair separation gives the lowest energy, as it gives the greatest  $V_{\delta}$ – $V_{\delta}$  separation, confirming the repulsive nature of pair–pair interaction.

In summary, comparing with the defect interactions in cubic YSZ, in tetragonal phase, Y atoms do not definitely have the largest separation in a Y– $V_{\delta}$ –Y trimer doping unit, but choose the smallest  $V_{\delta}$ –Y separation of larger attraction to partially compensate the Y–Y repulsion at shorter distances, such as the 11 [YY-1] configuration; oxygen vacancies form pairs along  $\langle 1, \frac{1}{2}, 0 \rangle$  at low concentration and transforms to the  $\langle 1, \frac{1}{2}, \frac{1}{2} \rangle$  direction at high Y concentration, which is correlated with the change of lattice parameters with the increasing Y concentration.

### 3.3. Correlation of microscopic defect configuration with macroscopic phase transition and lattice properties in cubic and tetragonal YSZ

From computational point of view, one reason for the existence of large controversies with respect to the defect–defect interactions and defect configurations in YSZ is because calculations are done with

different methods and different computational and system setups, and there is no good way to validate a given calculation result, especially the energy differences between different defect configurations are often very small in the same order of computational accuracy. Generally, the first-principles calculations suffer from limitations of system size and periodic boundary conditions. For ionic solids, the supercell size must be larger than the electrostatic screening length, typically in the order of a few nanometers for YSZ [41]. Periodic boundary conditions are restricted in treating real defect distributions which are random. Another difficulty is that direct comparison between the computations and experiments is limited because the microscopic experimental data of atomic defect configurations of YSZ are limited and sometimes non-conclusive. To circumvent these difficulties, we adopt here a different strategy to validate our computation results. We use the optimized microscopic atomic defect configurations as inputs to calculate the macroscopic properties of relative phase stability and lattice parameters of cubic and tetragonal YSZ as a function of Y concentration, then compare the resulting macroscopic properties with the experiments. These macroscopic properties are much easier to measure experimentally so that more abundant and reliable experimental data are available for comparison.

#### 3.3.1. Relative phase stability of cubic and tetragonal YSZ

In calculating the phase stability, we optimized all the cell parameters subject to the given lattice symmetry (i.e., cubic vs. tetragonal) and internal atomic coordinates subject to the given defect configurations (i.e., the lowest-energy ones). Fig. 2 shows the relative phase stability of cubic and tetragonal YSZ vs. Y concentration. The phase transition from tetragonal to cubic phase is predicted to occur at ~10% Y concentration with the increasing Y concentration, which is in good agreement with the experiment which reported that YSZ can be partially stabilized in the tetragonal phase at low Y concentration and fully stabilized in the cubic phase above 8% to 15% Y concentration [5].

At low Y concentration below the phase transition point (~10% Y concentration), the tetragonal phase is more stable because the pure  $ZrO_2$  favors the tetragonal phase. Above the transition point, the cubic phase becomes more stable, and the largest energy difference between the cubic and tetragonal phase occurs at 18.75% Y concentration, as shown in Fig. 2. We observe empirically an interesting correlation between the relative stability of cubic versus tetragonal phase and the difference of oxygen displacement between cubic and tetragonal YSZ, as shown in Fig. 3. The oxygen displacement ( $du$ ) in cubic YSZ is completely induced by doping and occurs equally along all three crystallographic directions. The oxygen displacement ( $dz$ ) in tetragonal YSZ is induced by both lattice distortion and doping and occurs dominantly along z-axis. We found that in cubic YSZ,  $du$  first increases and then decreases with the increasing Y concentration, while in tetragonal YSZ,  $dz$  decreases monotonically with the increasing Y concentration, as shown in Fig. 3A. In Fig. 3B, the difference

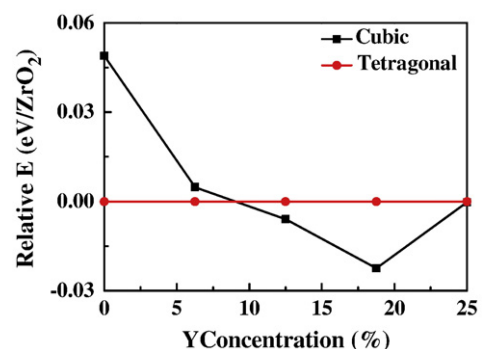
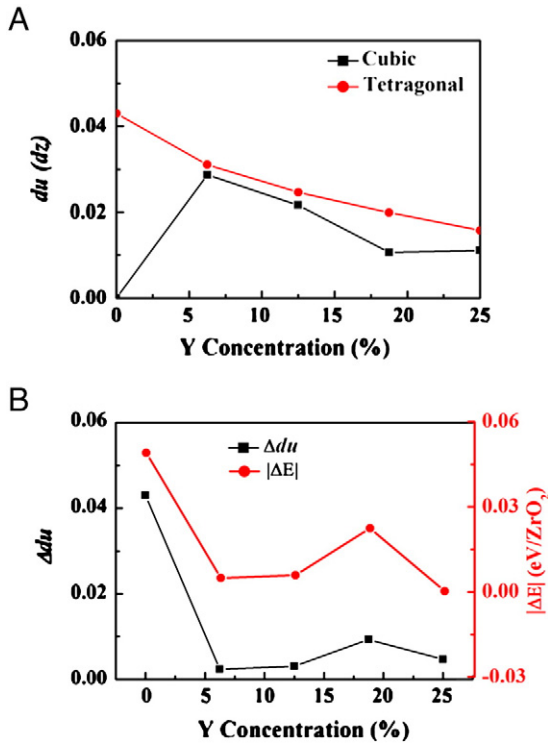


Fig. 2. Relative energy of cubic and tetragonal YSZ vs. Y concentration. The tetragonal phase is set as the reference of zero energy.



**Fig. 3.** (A) The internal parameter  $du$  in cubic and  $dz$  in tetragonal YSZ; (B) the difference in internal parameter  $\Delta du$  vs. Y concentration ( $\Delta du = dz(\text{tetragonal}) - du(\text{cubic})$ ) and  $|\Delta E| = |E(\text{tetragonal}) - E(\text{cubic})|$ .

of oxygen displacement ( $\Delta du$ ) and the absolute value of the difference of relative energy ( $|\Delta E|$ ) in cubic vs. tetragonal YSZ are plotted as a function of Y concentration, which shows that the energy difference between these two phases has a close correlation with the difference of oxygen displacement. As the  $\Delta du$  shows a minimum difference in the range of 6.25–12.5% Y concentration, the  $|\Delta E|$  displays also a minimum in about the same range of Y concentration where the phase transition occurs. Note that at high Y concentration of 25%, the energies of two phases become almost degenerate and the difference of oxygen displacements in the two phases is also very small. This is because at such high Y concentration, the tetragonal phase has a  $c/a$  ratio very close to 1.0 (see Fig. 4 below), becoming indistinguishable from the cubic phase. Experimentally, it has been observed that between 26% and 57% Y concentration [4], YSZ separates into a mixture of cubic YSZ and rhombohedra  $Y_4Zr_3O_{12}$  [42] and beyond 57% Y concentration, the  $Y_4Zr_3O_{12}$  phase dominates [4]. Our calculations suggest that the observed phase separation starting at ~25% Y concentration is possibly related to the fact of degenerate energy between the “tetragonal” and cubic phase at the 25% Y concentration and the cubic YSZ is not the solely stable phase at the high Y concentration.

### 3.3.2. Lattice properties of cubic and tetragonal YSZ

Next we analyze the changes of lattice parameters as a function of Y concentration for both cubic (single parameter,  $a$ ) and tetragonal (two parameters,  $a$  and  $c$ ) phases and compare our calculations with experiments. Fig. 4A shows that the lattice constant of the cubic phase increases almost linearly with the increasing Y concentration, with a linear fit of  $a = 5.049 + 0.233x$  in the range of  $0.0625 < x < 0.25$  (see solid line in Fig. 4A,  $x$  is the Y concentration), which is in good agreement with the experimental result of  $a = 5.104 + 0.204x$  ( $0.18 < x < 0.90$ ) [43]. This linear dependence indicates a uniform lattice expansion upon Y doping, which in turn suggests that doping is isotropic without any directional preference and defect distribution is completely random. This is because there is equal number of

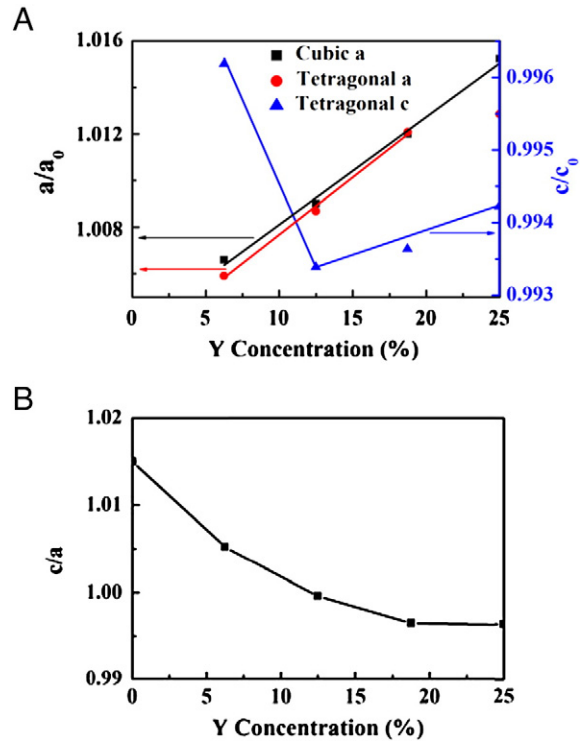


**Fig. 4.** (A) The lattice constants of cubic and tetragonal YSZ vs. Y concentration (in units of pure  $ZrO_2$  lattice constants,  $a_0$  and  $c_0$ ). The solid lines are the linear fits for the given Y concentration regimes; (B) the  $c/a$  vs. Y concentration in tetragonal YSZ.

equivalent alignments and directions along all three crystallographic axes in the cubic phase, although there are specifically favored alignments of oxygen vacancy pairs and directions of pair–pair interactions, as we discussed in section IIA. Consequently, the overall average doping effect has no directional preference, leading to isotropic doping and uniform lattice expansion.

The situation is different for the tetragonal phase because of the lower lattice symmetry. Fig. 4A shows that for the tetragonal YSZ, the lattice constant  $a$  increases with the increasing Y, with a linear fitting of  $a = 5.051 + 0.248x$  in the range of  $0.0625 < x < 0.1875$  (solid line in Fig. 4A), which agrees well with the experimental result in the same range of  $x$ ,  $a = 5.080 + 0.349x$  ( $0.05 < x < 0.13$ ) [43]. The lattice constant  $c$  first decreases, and then increases with the increasing Y concentration, and for the decreasing regime the linear fitting gives  $c = 5.107 - 0.229x$  ( $0.0625 < x < 0.125$ ), which is in good agreement with experimental result in the same range of,  $c = 5.195 - 0.309x$  ( $0.05 < x < 0.13$ ) [43]. For the increasing regime, the linear fitting gives  $c = 5.074 + 0.034x$  ( $0.125 < x < 0.25$ ). From the calculated lattice parameters  $a$  and  $c$ , we plotted the  $c/a$  ratio as a function of Y concentration in Fig. 4B, which shows that the  $c/a$  ratio decreases monotonically with the increasing Y concentration. By ~10% Y concentration where phase transition from tetragonal to cubic phases occurs, the  $c/a$  ratio of the tetragonal phase actually becomes very close to 1.0.

Below we try to understand why the lattice parameter  $c$  of the tetragonal phase first decreases and then increases with the increasing Y concentration. This intriguing behavior is found to be correlated with the microscopic atomic defect configurations which evolve in two different regimes of oxygen vacancy arrangements and interactions at different Y concentrations. At low Y concentration (below 12.5%), the oxygen vacancies align predominantly in the  $[1, \frac{1}{2}, 0]$  direction, rather than the  $[0, 1, \frac{1}{2}]$  or  $[1, 0, \frac{1}{2}]$  direction (note that these three directions would be equivalent in the cubic lattice). This implies that oxygen vacancies occupy the  $x$ - $y$  plane of oxygen atoms in the lattice, as shown in Fig. 5A, rather than the  $x$ - $z$  or  $y$ - $z$  plane of oxygen atoms. Because the concentration of oxygen vacancies is relatively low, they

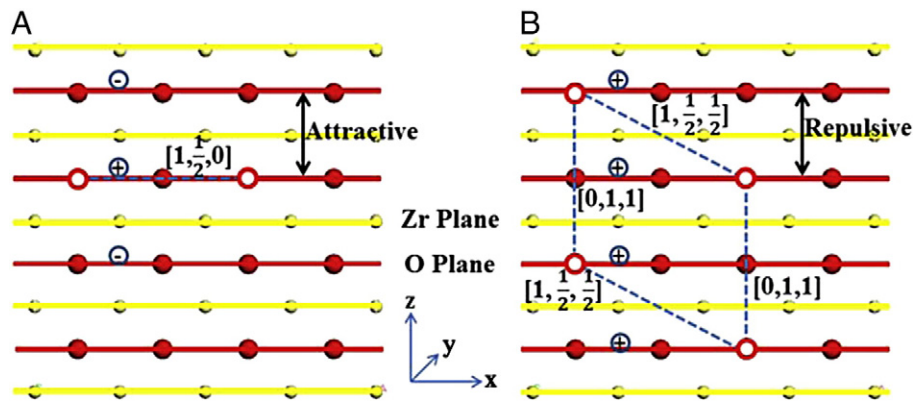


Fig. 5. (A) Low Y concentration oxygen vacancy alignment in tetragonal YSZ; (B) high Y concentration oxygen vacancy alignment in tetragonal YSZ. Zr/Y atoms are small (yellow) balls, oxygen atoms are large (red) balls, and oxygen vacancies are (red) open circles.

only appear in one of every few  $x$ - $y$  planes of oxygen. Notice that effectively, the  $x$ - $y$  plane of oxygen with vacancies will become positively charged, which causes a relatively “attractive” interaction between the vacancy-occupied oxygen plane and its neighboring oxygen planes without vacancy, i.e., their interaction becomes less repulsive than that between two oxygen planes without vacancy. Consequently, this effective attraction causes a shrinkage of lattice along  $z$ -direction and a decrease of lattice parameter  $c$  with the increasing Y concentration, as shown in Fig. 4A. One may argue that Y is expected to also have an effect on lattice due to its size and charge difference in replacing Zr. However, we found that Y atom does not have a strong site (alignment) preference as  $V_O$  does, as they occupy among different 2NN positions to  $V_O$ . Consequently, the size and charge effect of Y are close to be homogenous, expand the lattice more or less uniformly in all directions, so that it increases the lattice constant but without changing substantially the  $c/a$  ratio. For this reason, we attribute the change of  $c/a$  ratio mostly to the oxygen vacancy alignment.

In contrast, at high Y concentration (above 12.5%), the oxygen vacancies change to the  $[1, \frac{1}{2}, \frac{1}{2}]$  alignment. This implies that oxygen vacancies must occupy two neighboring  $x$ - $y$  planes simultaneously, as shown in Fig. 5B. So effectively, these two  $x$ - $y$  planes of oxygen with vacancies become positively charged, causing a relatively “repulsive” interaction between them in comparison to the situation of low Y concentration when only one isolated  $x$ - $y$  plane of oxygen vacancies is effectively positively charged. Consequently, this effective repulsion causes an expansion of lattice along  $z$ -direction and an increase of lattice parameter  $c$  with the increasing Y concentration, as shown in Fig. 4A.

The above analysis illustrates that the macroscopic lattice properties are closely correlated with the microscopic atomic defect configurations in YSZ. Furthermore, the defect configurations and interactions we found might shed some lights on explaining the experimentally observed ionic conductivity behavior. At low Y concentration (below 12.50%), oxygen vacancies are more mobile because individual  $V_O$  and  $V_O V_O$  pair within one single  $x$ - $y$  plane of oxygen, as shown in Fig. 5A, may jump within the same  $x$ - $y$  plane or to the neighboring  $x$ - $y$  planes of oxygen independently. At high Y concentration (above 25%), oxygen vacancies are less mobile because oxygen vacancies occupying simultaneously in two neighboring  $x$ - $y$  planes of oxygen, as shown in Fig. 5B, have to jump concertedly in a correlated manner to retain their low-energy  $[1, \frac{1}{2}, \frac{1}{2}]$  alignments. On the other hand, there are more oxygen vacancies available at high Y concentration than at low Y concentration. We speculate that the combination of two counteracting effects of oxygen vacancy mobility and concentration is partially responsible for the ionic conductivity have a maximum at 15%–18% Y concentration [5].

#### 4. Conclusions

We have performed a detailed first-principles study of atomic defect configurations in cubic and tetragonal YSZ as a function of Y concentration. In general, the defect configurations are found to be governed by the competition between the electrostatic interaction energies and strain energies, with the former being the most dominant effect, which are induced by different charge states and atomic sizes of the doped defects (ions and vacancies) from the host ions. At high Y concentrations, pairing and clustering of defects occur along preferred crystallographic directions that may vary with the increasing Y concentration to balance the change of electrostatic and strain energies. These changes in microscopic atomic defect configurations are shown to be closely correlated with the macroscopic properties of relative phase stability between the cubic and tetragonal phase of YSZ and their respective lattice properties. Such correlation also facilitates a direct comparison between our calculations and experiments, and provides an effective means to validate the computational results. Specifically, based on our optimized defect configurations, we correctly identified the tetragonal to cubic YSZ phase transition point and predicted the changes of lattice parameters with the increasing Y concentration, in good agreement with experiment.

#### Acknowledgments

We thank Christian Carbogno and Matthias Scheffler for their helpful discussions. And we are grateful for the financial support from DOE EFRC grant number DE-SC0001061 as a flow through from the University of South Carolina. We also thank DOE-NERSC and CHPC at the University of Utah for providing computing resources.

#### References

- [1] G. Teufer, Acta Crystallogr. 15 (1962) 1187.
- [2] O. Ruff, F. Ebert, Z. Anorg. Allg. Chem. 180 (1929) 19.
- [3] M. Yashima, K. Ohtake, M. Kakihana, H. Arashi, M. Yoshimura, J. Phys. Chem. Solids 57 (1996) 17.
- [4] C. Pascual, P. Duran, J. Am. Ceram. Soc. 66 (1983) 23.
- [5] M. Yashima, K. Morimoto, N. Ishizawa, M. Yoshimura, J. Am. Ceram. Soc. 76 (1993) 1745.
- [6] R. Krishnamurthy, Y.-G. Yoon, D.J. Srolovitz, R. Car, J. Am. Ceram. Soc. 87 (2004) 1821.
- [7] R. Devanathan, W.J. Weber, S.C. Singhal, J.D. Gale, Solid State Ionics 177 (2006) 1251.
- [8] J.P. Goff, W. Hayes, S. Hull, M.T. Hutchings, K.N. Clausen, Phys. Rev. B 59 (1998) 14202.
- [9] G. Stapper, M. Bernasconi, N. Nicoloso, M. Parrinello, Phys. Rev. B 59 (1999) 797.
- [10] C.R.A. Catlow, A.V. Chadwick, G.N. Greaves, L.M. Moroney, J. Am. Ceram. Soc. 69 (1986) 272.

- [11] D. Kmoyoji, A. Yoshiasa, T. Moriga, S. Emura, F. Kanamaru, K. Koto, *Solid State Ionics* 50 (1992) 291.
- [12] P. Li, I.-W. Chen, J.E. Penner-Hahn, *J. Am. Ceram. Soc.* 77 (1994) 118.
- [13] B.W. Veal, A.G. McKale, A.P. Paulikas, S.J. Rothman, L.J. Nowicki, *Physica B+C* 150 (1988) 234.
- [14] S. Ostanin, A.J. Craven, D.W. McComb, D. Vlachos, A. Alavi, A.T. Paxton, M.W. Finnis, *Phys. Rev. B* 65 (2002) 224109.
- [15] X. Xia, R. Oldman, R. Catlow, *Chem. Mater.* 21 (2009) 3576.
- [16] M.S. Khan, M.S. Islam, D.R. Bates, *J. Mater. Chem.* 8 (1998) 2299.
- [17] A. Eichler, *Phys. Rev. B* 64 (2001) 174103.
- [18] M. Weller, *Z. Metallkd.* 84 (1993) 381.
- [19] M.H. Tuilier, J. Dexpert-Ghys, H. Dexpert, P. Lagarde, *J. Solid State Chem.* 69 (1987) 153.
- [20] D. Steele, B.E.F. Fender, *J. Phys. C: Solid State Phys.* 7 (1974) 1.
- [21] W.L. Roth, R. Wong, A.I. Goldman, E. Canova, Y.H. Kao, B. Dunn, *Solid State Ionics* 18–19 (1986) 1115.
- [22] H. Morikawa, Y. Shimizugawa, F. Marumo, T. Harasawa, H. Ikawa, K. Tohji, Y. Udagawa, *J. Ceram. Soc. Jpn.* 96 (1988) 253.
- [23] A. Bogicevia, C. Wolverton, *Phys. Rev. B* 67 (2003) 024106.
- [24] K. Kawata, H. Maekawa, T. Nemoto, T. Yamamura, *Solid State Ionics* 177 (2006) 1687.
- [25] Z.R. Dai, Z.L. Wang, Y.R. Chen, H.Z. Wu, W.X. Liu, *Philos. Mag.* A 73 (1996) 415.
- [26] R. Osborn, N.H. Andersen, K. Clausen, M.A. Hackett, W. Hayes, M.T. Hutchings, J.E. MacDonald, *Mater. Sci. Forum* 7 (1986) 55.
- [27] S. Hull, T.W.D. Farley, M.A. Hackett, W. Hayes, R. Osborn, N.H. Andersen, K. Clausen, M.T. Hutchings, W.G. Stirling, *Solid State Ionics* 28–30 (1988) 488.
- [28] A. Bogicevic, C. Wolverton, G.M. Crosbie, E.B. Stechel, *Phys. Rev. B* 64 (2001) 014106.
- [29] A. Predith, G. Ceder, C. Wolverton, K. Persson, T. Mueller, *Phys. Rev. B* 77 (2008) 144104.
- [30] P. Dalach, D.E. Ellis, A. van de Walle, *Phys. Rev. B* 82 (2010) 144117.
- [31] V. Blum, R. Gehrke, F. Hanke, P. Havu, V. Havu, X. Ren, K. Reuter, M. Scheffler, *Comput. Phys. Commun.* 180 (2009) 2175.
- [32] V. Havu, V. Blum, P. Havu, M. Scheffler, *J. Comput. Phys.* 228 (2009) 8367.
- [33] J.P. Perdew, Y. Wang, *Phys. Rev. B* 45 (1992) 13244.
- [34] J.P. Perdew, K. Burke, M. Ernzerhof, *Phys. Rev. Lett.* 77 (1996) 3865.
- [35] X. Zhao, D. Vanderbilt, *Phys. Rev. B* 65 (2002) 075105.
- [36] B. Kralik, E.K. Chang, S.G. Louie, *Phys. Rev. B* 57 (1998) 7027.
- [37] C.J. Howard, R.J. Hill, B.E. Reichert, *Acta Crystallogr. B* 44 (1988) 116.
- [38] P. Aldebert, J.P. Traverse, *J. Am. Ceram. Soc.* 68 (1985) 34.
- [39] R.D. Shannon, *Acta. Cryst.* A32 (1976) 751.
- [40] S. Fabris, A. Paxton, M.W. Finnis, *Acta Mater.* 50 (2002) 5171.
- [41] J. Maier, *Prog. Solid State Chem.* 23 (1995) 171.
- [42] S.P. Ray, V.S. Stubican, D.E. Cox, *Mater. Res. Bull.* 15 (1980) 1419.
- [43] R.P. Ingel, D. Lewis III, *J. Am. Ceram. Soc.* 69 (1986) 325.